Journal of Alloys and Compounds 508 (2010) 152–157

Contents lists available at ScienceDirect

Journal of Alloys and Compounds

journal homepage: www.elsevier.com/locate/jallcom

Characterization of in situ α-Mo/Mo_5SiB_2 nanocomposite produced by mechanical alloying

A.R. Abbasi, M. Shamanian*

Department of Materials Engineering, Isfahan University of Technology, Isfahan 84156-83111, Iran

ARTICLE INFO

Article history:
Received 19 June 2010
Received in revised form 5 August 2010
Accepted 6 August 2010
Available online 19 August 2010

Keywords:
Nanocomposite
Mo_5SiB_2
Intermetallics
Mechanical alloying

ABSTRACT

The α-Mo/Mo_5SiB_2 nanocomposite was synthesized by mechanical alloying of the elemental powders. The structural evolutions of powder particles during mechanical alloying were studied by X-ray diffractometry, scanning electron microscopy and microhardness measurements. After 10 h of milling, a supersaturated solid solution of Si and B in Mo was formed and a composite microstructure consisting of fine boron and silicon particles distributed into molybdenum solid solution matrix was observed. In addition, the crystallite size of Mo reached to less than 23 nm. After 20 h of milling, new peaks related to Mo_5SiB_2 appeared in X-ray diffractograms. The microstructure of 20 h milled samples showed a composite structure in which intermetallic phases were embedded in a continuous α-Mo matrix. At this time, molybdenum crystallite size was 14 nm and a considerable increase in hardness value of powder particles was yielded due to the formation of Mo_5SiB_2. By further increase of milling time to 40 h, the molybdenum content of Mo_5SiB_2 increased whereas the crystallite size decreased. The 40 h milled powders had microhardness up to 1200 $HV_{0.1}$ due to refinement of crystallite size.

1. Introduction

High temperature processes are becoming more and more common in today's industrial society. With these processes comes the demand for superior materials that will extend the maximum operating temperature of components such as gas turbines, heat exchangers and heating elements [1]. Structural materials used in high temperature environments should have adequate strength, excellent oxidation resistance, superior creep resistance and good fracture toughness. In this regard, new materials have been developed to achieve all of these desired properties [2,3].

Molybdenum disilicide is of considerable interest due to its excellent oxidation resistance, high melting temperature, and relatively easy processing. Consequently, this compound is attractive candidate material for potential applications in high temperatures. However, $MoSi_2$ exhibits poor low temperature mechanical strength, unfortunate creep resistance at high temperatures and poor oxidation resistance at moderated temperature (600–800 °C) because of its 'pesting behavior' [4–7]. Therefore, the structural application of $MoSi_2$ has encountered some limitations.

Another silicide, Mo_5Si_3, is dynamically being investigated as a possible material for high temperature applications. Although, this material has superior creep resistance when compared to $MoSi_2$, but, the oxidation resistance of this compound is poor [8]. However, Meyer et al. [9–11] found that small additions (2 wt.%) of boron to Mo_5Si_3 can noticeably improve the isothermal oxidation behavior at high temperatures and can eliminate the pest oxidation at moderate temperatures.

When B is added to the Mo–Si system, Mo, Si, and B can form a ternary phase called T2 with a composition Mo_5SiB_2. T2 offers an attractive property balance of high melting temperature, oxidation resistance and useful high temperature mechanical properties [12,13]. Since it possesses a complex tetragonal structure (D8l-type structure), outstanding creep resistance is expected for this compound at ultra-high temperatures [14]. It was reported that the single crystal of Mo_5SiB_2 exhibits some deformability and extremely high strength at 1773 K in certain orientations [15–18]. Ito et al. [18] investigated high temperature strength and creep properties of Mo_5SiB_2 single crystal. They showed that it has greater excellent high temperature strength than that of $MoSi_2$ and Mo_5Si_3 single crystals and their composites [18,19]. T2 is believed to provide excellent oxidation resistance from the boron-added silica glass scale that forms when it is oxidized [3,20]. Therefore, Mo_5SiB_2 is a new, highly potential candidate for ultra-high temperature applications. But the major challenge still lies in the inherent brittleness of Mo_5SiB_2 [3].

An optimum combination of room temperature fracture toughness, high temperature creep and oxidation resistance possibly can be achieved by using a microstructure in which Mo_5SiB_2 is dispersed in a ductile α-Mo phase [21–23]. A further improvement of

* Corresponding author. Tel.: +98 311 3915737; fax: +98 311 3915737.
E-mail address: shamanian@cc.iut.ac.ir (M. Shamanian).

0925-8388/$ – see front matter © 2010 Elsevier B.V. All rights reserved.
doi:10.1016/j.jallcom.2010.08.036

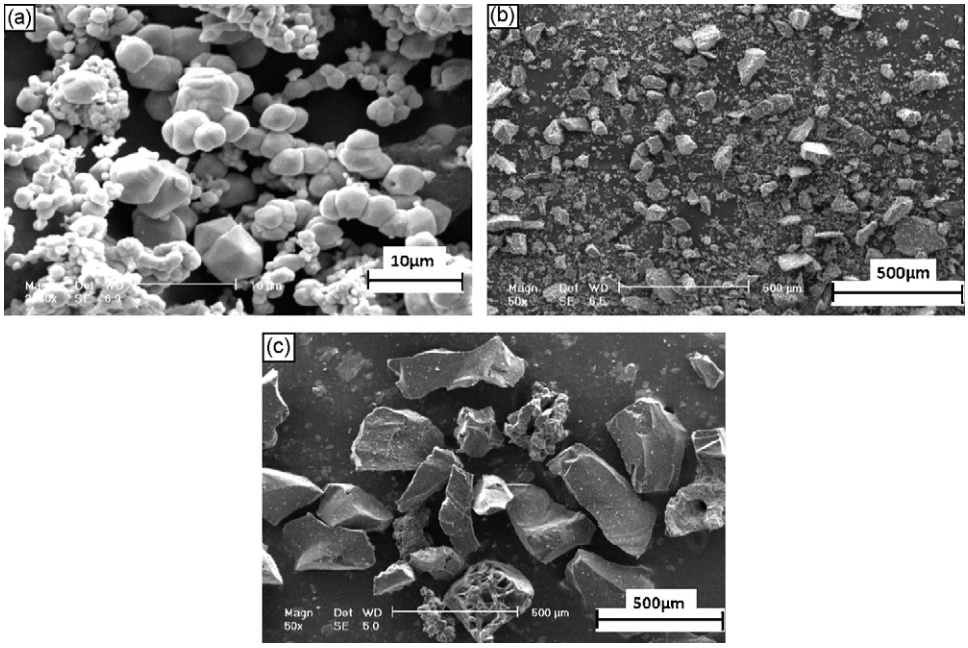

Fig. 1. Secondary electron SEM micrographs of as-received elemental powder particles: (a) Mo, (b) Si and (c) B.

mechanical properties can be achieved by decreasing of the grain size to the nanometer scale.

The formation of alloys via solid-state reaction that occurs during ball milling of elemental powders, called mechanical alloying (MA), is a useful way for production of such nanocomposites [24–27]. During MA both matrix and reinforcement are formed through an in situ process, which will promote good bonding between matrix and reinforcement. Moreover, a homogeneous distribution of fine reinforcing particles can be obtained by the MA process [28].

The synthesis of nanocrystalline alloys and intermetallic compounds by ball milling has been successfully achieved by several researchers [29–33].While many studies on MA for the Mo–Si binary system [34–39] have been reported, there is very little information about the synthesis of the Mo–Si–B ternary system by MA process.

In this work, the in situ synthesis of α-Mo/Mo_5SiB_2 nanocomposite was investigated by mechanical alloying. The phase transformations, structural and morphological evolutions occurring in MA process were also investigated.

2. Experimental procedure

The elemental powders of Mo (99.7 wt.% purity), Si (99.8 wt.% purity) and B (99 wt.% purity) were used as starting materials. Fig. 1 shows the secondary electron micrographs of elemental Mo, Si and B powder particles. The Mo particles were nearly uniform in size (~3 μm) with a spherical morphology. Si particles had an irregular shape with a size distribution of 5–100 μm and B particles had irregular shape with a size distribution of 100–300 μm.

The Mo, Si and B powders with molar ratio of 5:1:2 were mixed according to stoichiometric composition of Mo_5SiB_2. MA process was carried out in a high energy planetary ball mill, nominally at room temperature under Ar atmosphere. The milling media consisted of nine 20 mm diameter balls confined in a 250 ml volume vial. In this regard, hardened steel vials and balls were used for ball milling. The ball-to-powder weight ratio and milling speed were 15:1 and 300 rpm, respectively. The total powder mass was 20 g with 0.3 wt.% stearic acid as a process control agent (PCA) to prevent the agglomeration of powders during milling. Samples were taken at selected time intervals and characterized by X-ray diffraction (XRD) in a Philips X' PERT MPD diffractometer using filtered Cu K_α radiation (λ = 0.1542 nm). The crystallite size and internal strain of powders were estimated using the Williamson–Hall method [40]:

$$\beta \cos\theta = \frac{k\lambda}{d} + 2A\varepsilon \sin\theta$$

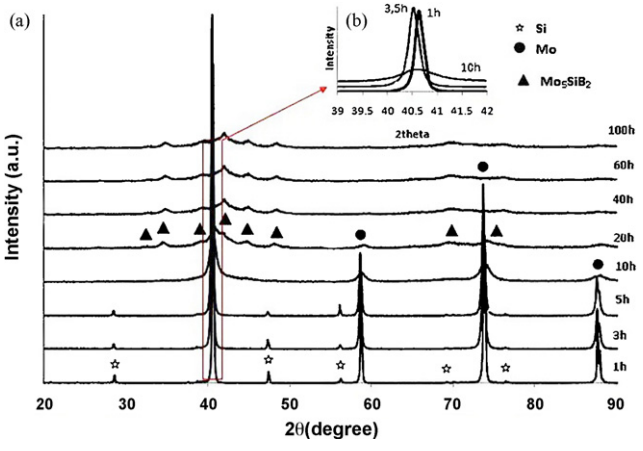

Fig. 2. X-ray diffractograms of powder mixture after different milling times (a). Insert shows the displacement of (1 1 0) Mo peak (b).

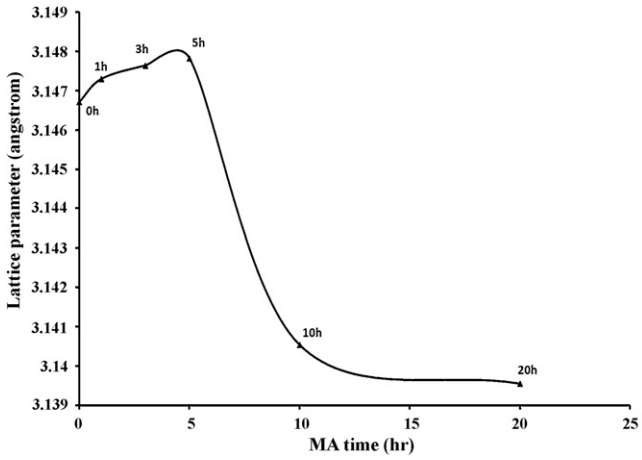

Fig. 3. Change of lattice parameter of Mo with milling time.

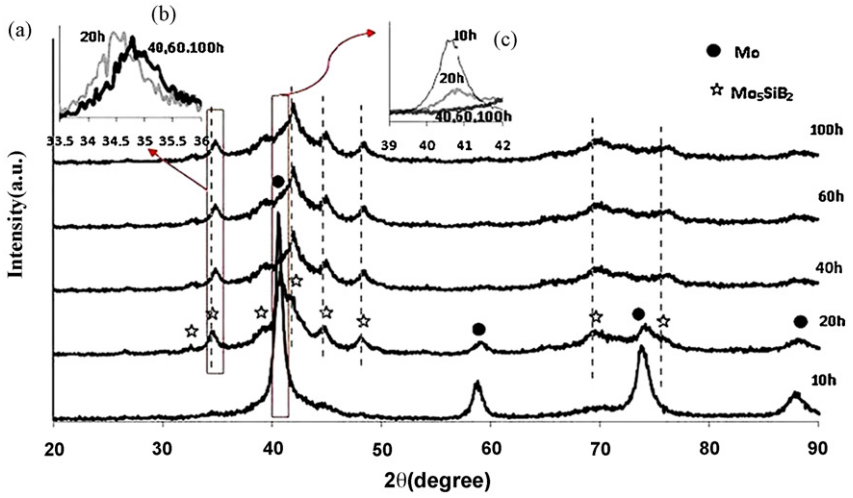

Fig. 4. (a) XRD patterns of powder mixture just before and after formation of T2. Inserts show variation of molybdenum intensity with increasing milling time (b) and the displacement of Mo_5SiB_2 peak (c).

where θ is the Bragg diffraction angle, D the crystallite size, ε the average internal strain, λ the wavelength of the radiation used, β the diffraction peak width at half maximum intensity, K the Scherrer constant (0.91) and A is the coefficient which depends on the distribution of strain; it is near to unity for dislocations.

Morphology and microstructure of powder particles were characterized by SEM in a Philips XL30 at an accelerating voltage of 30 kV. The mean powder particle size was estimated from SEM images of powder particles by image tool software. The average size of about 50 particles was calculated and reported as mean powder particle size. For measurement of microhardness, a small amount of powder particles was mounted. Prior to indentation, the surfaces of samples were polished using a sequence of increasing grit sandpaper followed by a series of diamond pastes. The Vickers microhardness at the polished cross-section of powders was measured with a microhardness tester at a load of 100 g and dwell time of 10 s. Ten Vickers indentation marks were performed on each sample.

3. Results and discussion

3.1. Structural evolution

Fig. 2 shows X-ray diffractograms of Mo–12.5 mol% Si–25 mol% B powder mixture after different milling times. After 1 h of milling, the diffraction pattern shows strong Mo peaks with relatively weak and broad Si peaks and B peaks cannot be displayed because of high mass absorption coefficient of Mo. The intensity of Si diffraction peaks decreases with increasing milling time. Increasing milling time to 10 h led to complete disappearance of Si peaks. The reduction in the intensity of the Si peaks is commonly observed during mechanical alloying of Mo–Si which can be attributed to the intimate mixing of the two elements, the strong absorption of Mo and dissolution of Si into Mo lattice during mechanical alloying [41–43].

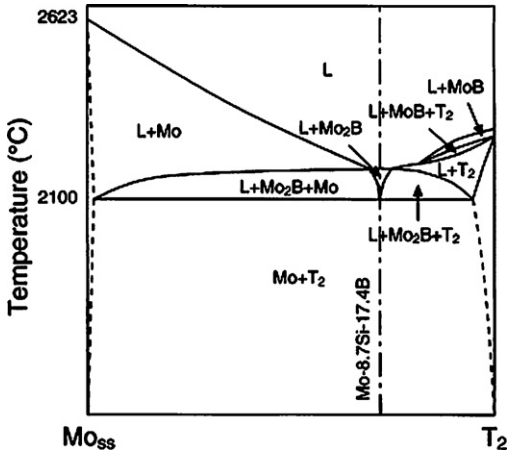

Fig. 5. Mo–Mo_5SiB_2 (T2) pseudo binary phase diagram [19].

Furthermore, during MA from 1 to 5 h, Mo peaks shift toward lower angles and after that Mo peaks shift to higher angles with increasing milling time from 5 to 10 h (Fig. 2b). The displacement of Mo peaks toward lower or higher angles can be related to lattice expansion or contraction. The lattice parameter of Mo in powder mixture was determined at different milling times by using Nelson–Riley function [44]. The effect of milling time on the lattice parameter of Mo has been shown in Fig. 3. Primarily, a gradual increase in Mo lattice parameter is observed which reaches a maximum value after 5 h, then, it decreases rapidly. The atomic radii of carbon, nitrogen, hydrogen, and boron are lower than 2 Å, so, an interstitial solid solution can be formed between a metal and one of these elements [44]. Here, an interstitial solid solution of B in Mo is expected to be formed. The interstitial addition of B to Mo is always accompanied by an increase in the volume of the unite cell. The increase in lattice parameter of Mo leads to shift of Mo peaks to lower angles. Thus, it can be suggested that B has been dissolved in Mo with increasing milling time from 1 to 5 h. With increasing milling time from 5 to 10 h, the lattice parameter of Mo decreases rapidly. The decrease in lattice parameter could be attributed to substitutional dissolution of Si atoms in Mo lattice. Since Si has significantly smaller atomic radius than Mo, the lattice parameter of Mo decreases by alloying with Si. The formation of substitutional solid solution of Si in Mo has been reported in the literature [37,43,50]. According to mentioned discussions, it can be concluded that Mo(Si,B) solid solution can be formed after 10 h of milling.

In the ternary Mo–Si–B phase diagram at 1600 °C, reported by Nunes et al. [45], α-Mo contains about 1 at.% B and 2–3 at.% Si [46]. However, Sakidja and Perepezko [46,47] have recently reported that solubility of B in Mo is negligible. On the other hand, Schneibel [48] has reported the presence of 3.2 at.% B in the α-Mo phase in the arc-melted ingots of Mo–19.5W–12Si–8.5B alloy can be due to the effect of W in formation of solid solution with Mo. It should be noted that solubility limit of B in α-Mo is still under investigation. The solid solubility limit of B and Si in Mo can be extended as a result of MA process leading to the formation of a supersaturated solid solution of Si and B in Mo due to the high dislocation density, large amounts of structural defects and the local stresses produced during MA.

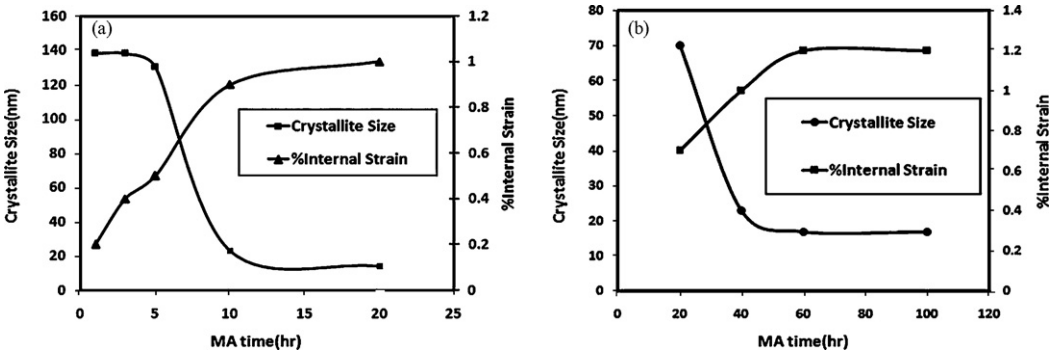

Fig. 6. Variation of crystallite size and internal strain of Mo (a) and Mo_5SiB_2 (b) with increasing milling time.

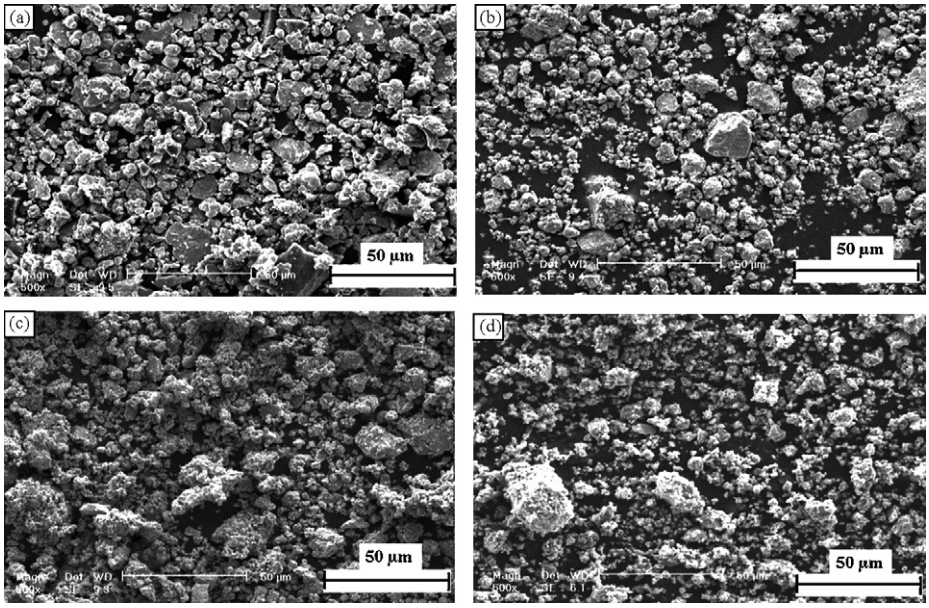

Fig. 7. X-ray diffractograms of powder mixture after different milling times (a) Insert shows the displacement of Mo(1 1 0) peak (b).

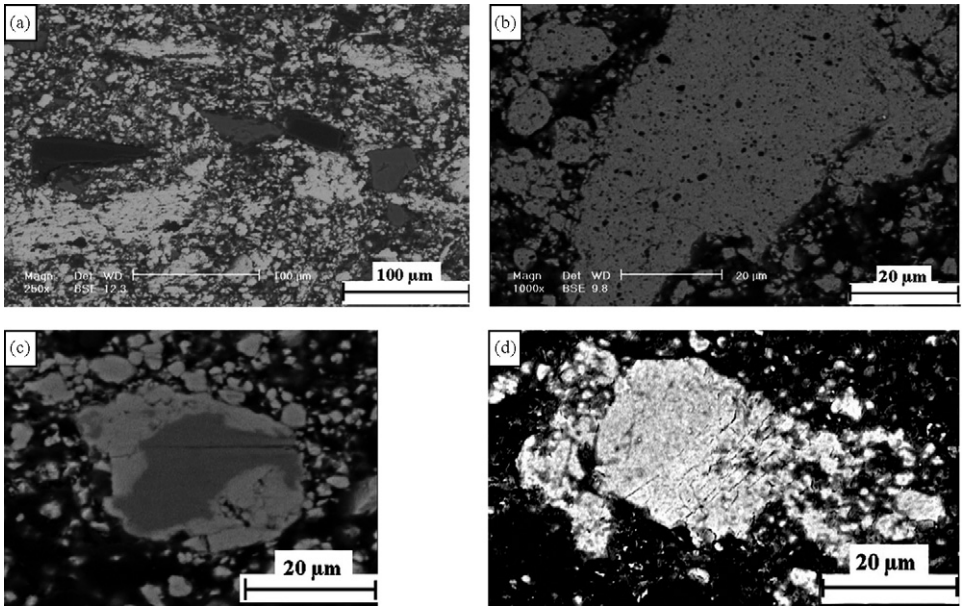

Fig. 8. Cross-sectional SEM images of powder mixture after (a) 5, (b) 10, (c) 20 and (d) 100 h of milling times.

Fig. 4 shows X-ray diffractograms of powder mixture just before and after formation of Mo_5SiB_2. After 10 h of milling, only Mo peaks are seen. With increasing milling time to 20 h, new peaks related to Mo_5SiB_2 appeared. Also, broadening of Mo peaks and decreasing of its intensity are seen. Further increasing of milling time led to broadening of Mo and Mo_5SiB_2 peaks due to the decreasing of their grain size and increasing of lattice strain during MA. After 40 h, the intensity of Mo peaks approximately reaches to zero (Fig. 4c). Moreover, during ball milling from 20 to 100 h, Mo_5SiB_2 peaks shift toward higher angles (Fig. 4b). This indicates that a quantity of Mo is dissolved into the lattice of Mo_5SiB_2 and Mo content of Mo_5SiB_2 is increased. Fig. 5 shows phase diagram of Mo–Mo_5SiB_2. It can be seen that Mo can dissolve in Mo_5SiB_2 and the Mo content in Mo_5SiB_2 decreases with decreasing temperature. It has been reported in the literature that the high dislocation density, large amounts of structural defects and the local stresses produced during MA can enhance solid solubility. Therefore, the solubility of Mo in Mo_5SiB_2 can increase by mechanical alloying.

The direct formation of α-Mo/Mo_5SiB_2 during milling process has not been reported yet. Although Yamauchi et al. [49] reported the formation of Mo_5SiB_2 by combination process of mechanical alloying and spark plasma sintering but they could not obtain this phase by mechanical alloying. Furthermore, they could not obtain α-Mo/Mo_5SiB_2 by mechanical alloying. Kurger et al. [50] had investigated formation of α-Mo–Mo_5SiB_2–Mo_3Si by mechanical alloying. They could not achieve this composite by mechanical alloying and only after consolidation they obtained the composite.

The crystallite size and the internal strain of Mo and Mo_5SiB_2 phases were obtained from XRD analysis using the Williamson–Hall method. In this method, both broadening contributions, due to the strain and crystallite size, are taken into account.

The crystallite size and internal strain of the Mo and Mo_5SiB_2 calculated from the line width are shown in Fig. 6 as a function of MA time. Three parts are seen in Fig. 6a. At early stages of milling, crystallite size of Mo does not change with increasing milling time but internal strain changes very slowly. With increasing milling time from 5 to 10 h, the crystallite size of Mo rapidly decreases and it receives to less than 23 nm after 10 h of MA. Also, the internal strain increases quickly to a high value of about 0.9% after 10 h of MA. Further refinement of the crystallite size occurs gradually to 14 nm after 20 h of MA and the strain approaches a steady-state value of 1% at this time. The Mo_5SiB_2 phase after 20 and 40 h milling times had a crystallite size of 70 and 23 nm and a lattice strain of 0.7% and 1%, respectively. Further refinement of the crystallite size occurs gradually to 17 nm after 60 h of MA and the strain approaches a steady-state value of 1.2% at this time.

3.2. Morphological changes

SEM images of powder particles after different milling times are shown in Fig. 7. After 5 h of milling (Fig. 7a), uniform distribution of small and large particles is seen. Smaller particles have equiaxed morphology with mean particle sizes of 2 μm. The larger particles have irregular shapes with smooth surface and their particle size is about 15 μm. Smooth surface of large particles indicates that these particles are created from brittle fracture of larger particles. Boron and silicon elemental powders had irregular morphology with very large particle sizes and molybdenum powders had spherical morphology with particle sizes of 3 μm. The comparison of morphology and size of elemental powders and milling powders confirms that only fracture of powder particles has occurred during milling up to 5 h and particle sizes of boron and silicon powders have decreased sharply. After 10 h of milling (Fig. 7b), particles have uniform shapes with non-uniform size distribution. Both small and large particles are seen but fraction of small particles is more. Similar shapes of all particles and 3D shapes of large particles indicate that cold welding process between powders and fracturing of powder particles occur with increasing milling time. The Cold welding process led to the formation of large particles with similar shapes and then a number of these large particles are broken. After 20 h of milling (Fig. 7c), agglomeration of powders is the main phenomenon. Particles have similar shapes. Similar to earlier, a distribution of small and large particles is seen. Large particles in this stage are in fact an agglomeration of many smaller particles. X-ray diffractograms showed that α-Mo/Mo_5SiB_2 composite formed after 20 h of milling. In this composite, α-Mo is matrix and Mo_5SiB_2 is reinforcement. α-Mo can act as a binder between different particles and therefore, agglomeration of powders take place. Increasing milling time to 100 h led to the formation of small and uniform particles (Fig. 7d).

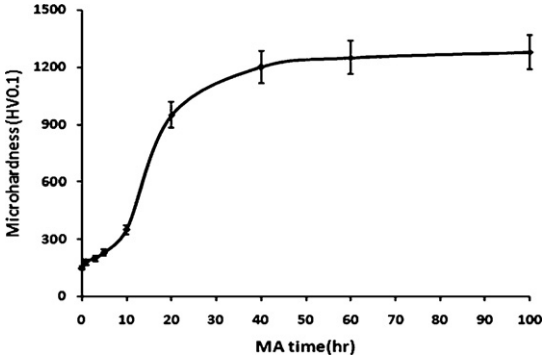

Fig. 9. Microhardness values of powder mixture as a function of MA time.

3.3. Microstructural observations

Fig. 8 shows cross-sectional SEM images of powder particles after different milling times. As can be seen, no composite or lamellar microstructure is seen at early stages of milling and elemental powders clearly are seen (Fig. 8a). Since back scatter (BS) signals are correlated to the atomic number of elements, bright, grey and dark areas in SEM images correspond to Mo, Si and B respectively. After 10 h of milling time, a composite microstructure consisting of cold welded Mo, Si and B phases is formed (Fig. 8b). This composite has the fine and uniform microstructure comprising fine boron and silicon particles distributed into molybdenum matrix. This composite microstructure is a result of repeated cold welding and fracturing of powder particles. This fine microstructure includes an extensive interface area between Mo, Si and B phases which promotes the interdiffusion of atoms through high diffusivity paths (dislocations and grain boundaries) and therefore, can increase the formation kinetics of Mo_5SiB_2 at ambient temperature. After 20 h of milling, Mo_5SiB_2 phase is formed. The microstructure of the powder particles consists of the desired distribution of the intermetallic particles in a continuous α-Mo matrix (Fig. 8c). Investigation by X-ray diffraction analyses proofs that Mo_5SiB_2 phase forms at this time. At longer milling times a featureless microstructure is observed on SEM (Fig. 8d) indicating that α-Mo/Mo_5SiB_2 nanocomposite is completely formed in consistence with XRD results.

3.4. Microhardness measurements

Fig. 9 shows the average value of microhardness of Mo–Si–B powder particles after different milling times. After 20 h of milling time a considerable increase in hardness value of powder particles is yielded. This increase in hardness value is due to the formation of Mo_5SiB_2 phase, consistent with XRD results. Refinement of grain size after 40 h of milling time increases the microhardness value to 1200 HV.

4. Conclusion

Mechanical alloying of Mo–12.5 mol% Si–25 mol% B powders leads to the synthesis of α-Mo/Mo_5SiB_2 nanocomposite. The formation mechanism of this nanocomposite can be envisaged as follows. At early stages of milling, an interstitial solid solution of B in Mo is formed and further milling leads to substitutional dissolution of Si in Mo. Therefore, after 10 h of milling, a solid solution of Si and B in Mo is formed and a composite microstructure consisting of fine boron and silicon particles distributed into molybdenum solid solution matrix is observed. This fine microstructure includes an extensive interface area between Mo, Si and B phases which promotes the interdiffusion of atoms through high diffusivity paths and therefore, can decrease the activation energy of formation of Mo_5SiB_2 at ambient temperature. This leads to formation of α-Mo/Mo_5SiB_2 nanocomposite after 20 h milling time.

References

[1] E. Summers, A.J. Thom, B. Cook, M. Akinc, Intermetallics 8 (2000) 1169–1174.
[2] S. Bose, Mater. Sci. Eng. A 155 (1992) 217–225.
[3] V. Supatarawanich, D.R. Johnson, C.T. Liu, Mater. Sci. Eng. A 344 (2003) 328–339.
[4] Y. Liu, G. Shao, P. Tsakiropoulos, Intermetallics 8 (2000) 953–962.
[5] J.J. Petrovic, A.K. Vasudevan, Mater. Sci. Eng. A 261 (1999) 1–5.
[6] N. Sekido, R. Sakidja, J.H. Perepezko, Intermetallics 15 (2007) 1268–1276.
[7] Y.Q. Liu, G. Shao, P. Tsakiropoulos, Intermetallics 9 (2001) 125–136.
[8] M.K. Meyer, M.J. Kramer, M. Akinca, Intermetallics 4 (1996) 273–281.
[9] M.K. Meyer, M. Akinc, J. Am. Ceram. Soc. 79 (1996) 2763–2766.
[10] M.K. Meyer, M. Akinc, J. Am. Ceram. Soc. 79 (1996) 938–944.
[11] M.K. Meyer, A.J. Thom, M. Akinc, Intermetallics 7 (1999) 153–162.
[12] F. Wang, A. Shan, X. Dong, J. Wu, J. Alloys Compd. 462 (2008) 436–441.
[13] R. Sakidja, J.H. Perepezko, S. Kim, N. Sekido, Acta Mater. 56 (2008) 5223–5244.
[14] K. Yoshimi, S. Nakatani, T. Suda, S. Hanada, H. Habazaki, Intermetallics 10 (2002) 407–414.
[15] K. Ihara, K. Ito, K. Tanaka, M. Yamaguchi, Mater. Sci. Eng. A 329–331 (2002) 222–227.
[16] C.J. Rawn, J.H. Schneibel, C.M. Hoffmann, C.R. Hubbard, Intermetallics 9 (2001) 209–216.
[17] H. Choe, D. Chen, J.H. Schneibel, R.O. Ritchie, Intermetallics 9 (2001) 319–329.
[18] K. Ito, K. Ihara, K. Tanaka, M. Fujikura, M. Yamaguchi, Intermetallics 9 (2001) 591–602.
[19] K. Yoshimi, S. Nakatani, N. Nomura, S. Hanada, Intermetallics 11 (2003) 787–794.
[20] F.A. Rioult, S.D. Imhoff, R. Sakidja, J.H. Perepezko, Acta Mater. 57 (2009) 4600–4613.
[21] S. Paswan, R. Mitra, S.K. Roy, Intermetallics 15 (2007) 1217–1227.
[22] J.H. Schneibel, M.J. Kramer, D.S. Easton, Scr. Mater. 46 (2002) 217–221.
[23] J.J. Kruzic, J.H. Schneibel, R.O. Ritchie, Scr. Mater. 50 (2004) 459–464.
[24] C.C. Koch, J. Mater. Sci. 42 (2007) 1403–1414.
[25] B.S.B. Reddy, K. Das, S. Das, J. Mater. Sci. 42 (2007) 9366–9378.
[26] L.Z. Zhou, J.T. Guo, G.J. Fan, Mater. Sci. Eng. A 249 (1998) 103–108.
[27] T. Yamasaki, Y.J. Zheng, Y. Ogino, M. Terasawa, T. Mitamura, T. Fukami, Mater. Sci. Eng. A 350 (2003) 168–172.
[28] C.C. Koch, Mater. Sci. Eng. A 244 (1998) 39–48.
[29] S.S. Nayak, M. Wollgarten, J. Banhart, S.K. Pabi, B.S. Murty, Mater. Sci. Eng. A 527 (2010) 2370–2378.
[30] H.H. Sheu, L.C. Hsiung, J.R. Sheu, J. Alloys Compd. 469 (2009) 483–487.
[31] J. Joardar, S.K. Pabi, B.S. Murty, J. Alloys Compd. 429 (2007) 204–210.
[32] A. Vyas, K.P. Rao, Y.V.R.K. Prasad, J. Alloys Compd. 475 (2009) 252–260.
[33] M.T. Marques, A.M. Ferraria, J.B. Correia, A.M. Botelho do Rego, R. Vilar, Mater. Chem. Phys. 109 (2008) 174–180.
[34] P.C. Kang, Z.D. Yin, O. Celestine, Mater. Sci. Eng. A 395 (2005) 167–172.
[35] L. Liu, K. Cui, J. Mater. Process. Technol. 138 (2003) 394–398.
[36] T. Schubert, A. Bohm, B. Kieback, M. Achtermann, R. Scholl, Intermetallics 10 (2002) 873–878.
[37] K. Zuo, S. Xi, J. Zhou, Mater. Sci. Eng. A 445 (2007) 48–53.
[38] P.V. Krakhmalev, Int. J. Refract. Met. H 22 (2004) 205–209.
[39] C. Suryanarayana, Mater. Sci. Eng. A 479 (2008) 23–30.
[40] G.K. Williamson, W.H. Hall, Acta. Metall. Mater. 1 (1953) 22–31.
[41] A.J. Heron, G.B. Schaffer, Mater. Sci. Eng. A 352 (2003) 105–111.
[42] L. Liu, F. Padella, W. Guo, M. Magini, Acta Metall. Mater. 43 (1995) 3755–3761.
[43] H. Zhang, X. Liu, Int. J. Refract. Met. H 19 (2001) 203–208.
[44] B.D. Cullity, Elements of X-ray Diffraction, 2nd ed., Addison-Wesley, 1978.
[45] C.A. Nunes, R. Sakidja, J.H. Perepezko, in: M.V. Nathal, R. Darolia, C.T. Liu, P.L. Martin, D.B. Miracle, R. Wagner, M. Yamaguchi (Eds.), Structural Intermetallics, TMS, Warrendale, PA, 1997, pp. 831–839.
[46] S. Kim, R. Sakidja, Z. Dong, J.H. Perepezko, Y.W. Kim, in: J.H. Schneibel, S. Hanada, K.J. Hemker, R.D. Noebe, G. Sauthoff (Eds.), High Temperature Ordered Intermetallic Alloys IX, MRS, Pittsburgh, PA, 2001, N5.42.1.
[47] R. Sakidja, J.H. Perepezko, Metall. Mater. Trans. A 36 (2005) 507–514.
[48] J.H. Schneibel, Intermetallics 11 (2003) 625–632.
[49] A. Yamauchi, K. Yoshimi, K. Kurokawa, S. Hanada, J. Alloys Compd. 434/435 (2007) 420–423.
[50] M. Kruger, S. Franz, H. Saage, M. Heilmaier, J.H. Schneibel, P. Jehanno, M. Boning, H. Kestler, Intermetallics 16 (2008) 933–941.